Heterogeneous Roughness Properties of Fault Surfaces: New Insights from Laboratory Experiments

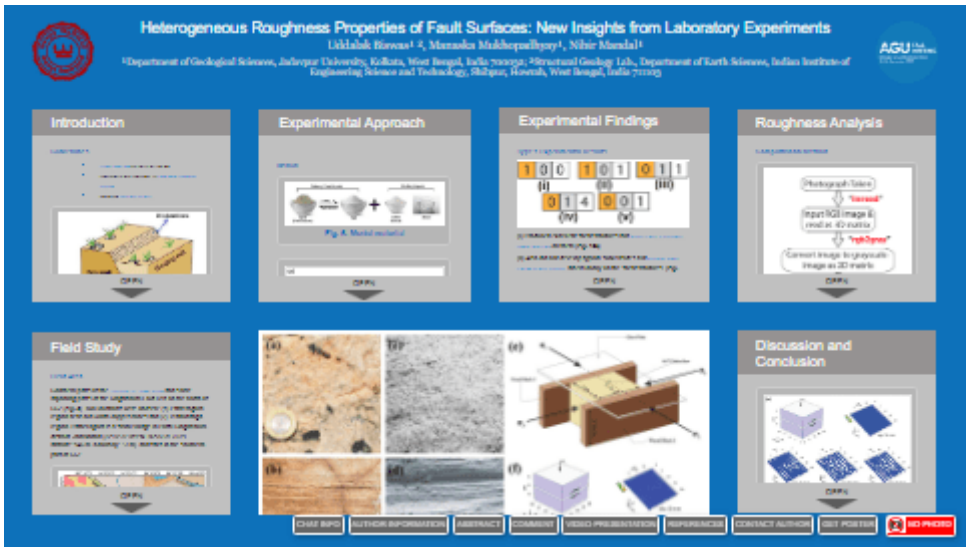

Uddalak Biswas[1] [2], Manaska Mukhopadhyay[1], Nibir Mandal[1]

[1]Department of Geological Sciences, Jadavpur University, Kolkata, West Bengal, India 700032; [2]Structural Geology Lab., Department of Earth Sciences, Indian Institute of Engineering Science and Technology, Shibpur, Howrah, West Bengal, India 711103

AGU FALL MEETING
Chicago, IL & Online Everywhere
12–16 December 2022

PRESENTED AT:

INTRODUCTION

Slickenlines

- Linear features on fault surfaces
- Geometrically defined by alternate ridge and groove
- Reliable indicator of slip

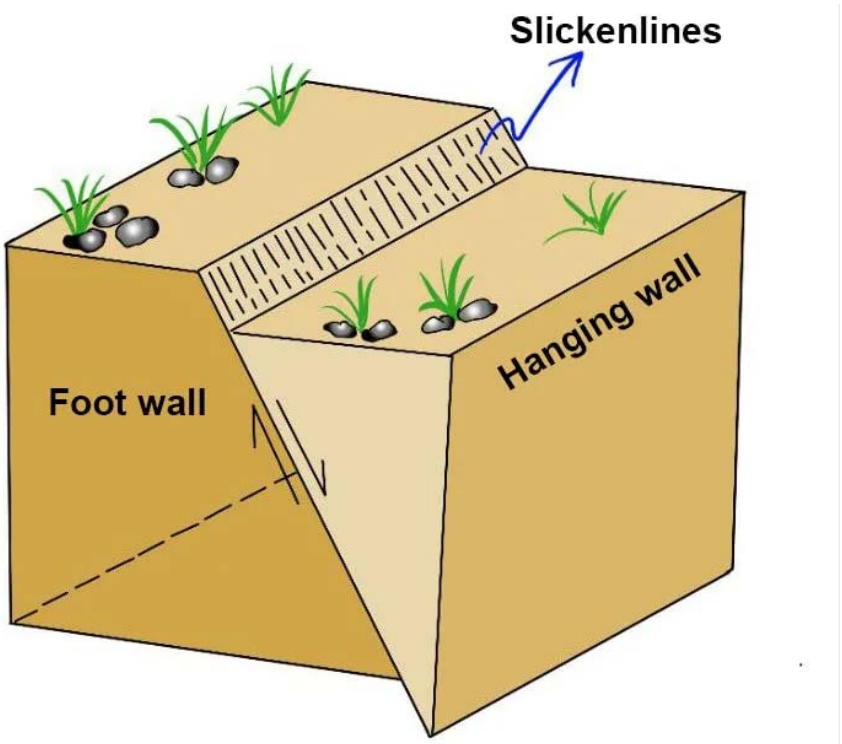

Fig. 1: Schematic diagram of slickenlines on the fault surface

Genetic types of classical slickenlines

Twiss and Moores (1992) **have classified slickenlines broadly into three types:**

- **Structural slickenlines originate from mechanical wearing and ploughing by hard asperities on relatively softer substrates. (*Fig. 2b*)**
- **Mineral slickenlines result from the accumulation of streaks from the smearing out of mineral grains or soft asperities behind hard asperities. (*Fig. 2d*)**
- **Fault movements often generate locally positive and negative dilation zones in the neighbourhood of geometrical irregularities. At the opening (positive dilation) locale, slickenfibers grow, tracking the local displacement vectors. (*Fig. 2e and f*)**

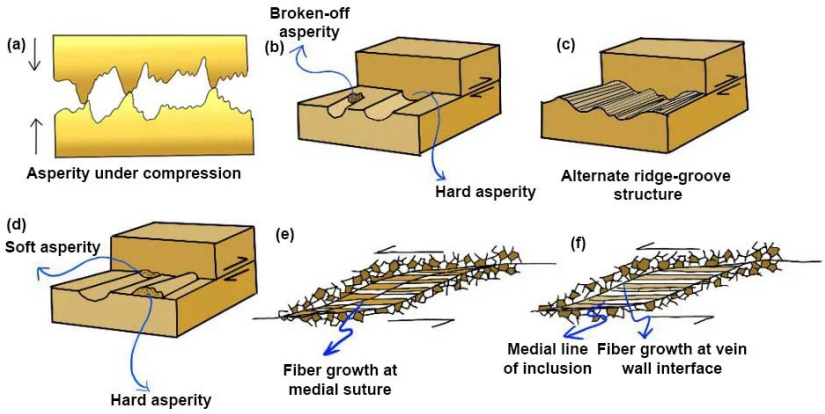

Fig. 2: Schematic diagram of (a) Asperity, (b) Structural slickenlines, (c) Slickenlines defined by alternate ridge and grooves, (d) Mineral slickenlines, (e) Syntaxial fiber slickenlines, (f) Antitaxial fiber growth. (Modified after *Twiss and Moores, 1992*)

EXPERIMENTAL APPROACH

Method

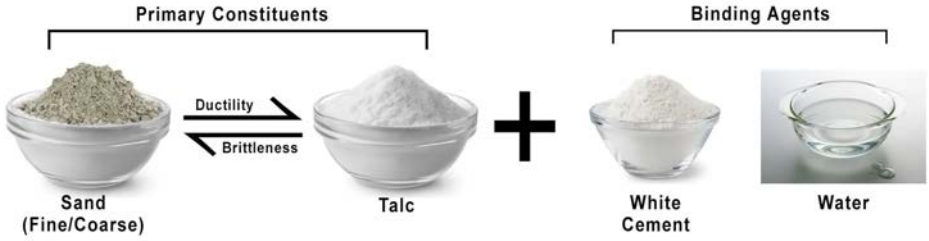

Fig. 6: Model material

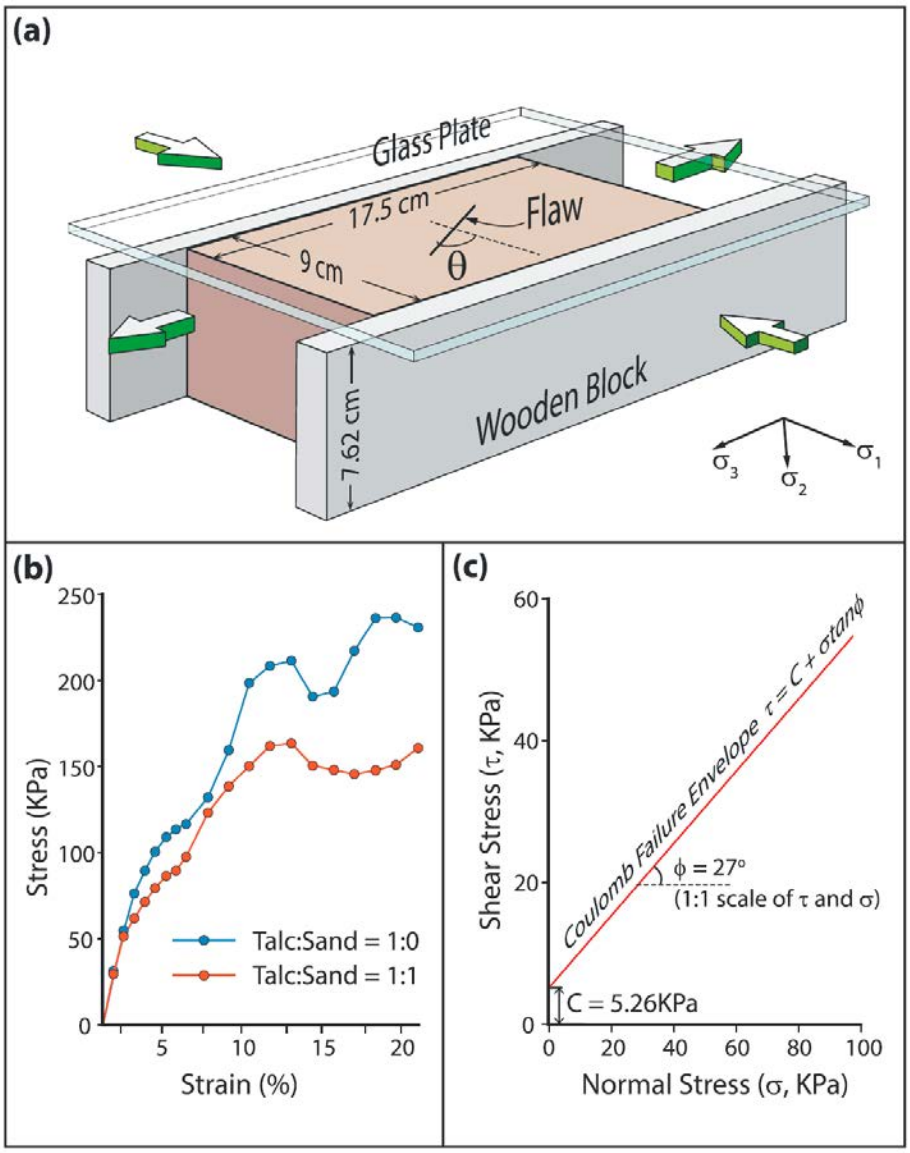

Fig. 7: (a) Laboratory setup for pure shear experiments with sand-talc models. (b) Yield behaviour of pure talc (blue) and sand-talc (1:1, orange) models under triaxial stress conditions. The major plastic failure occurred at 200 and 155 kPa, respectively, followed by stress drops. (c) Estimated Coulomb failure envelope for pure sand models.

- **Type 1 Model: This experiment had a small initial planar flaw (vertical planar cut with a length of 2 cm) in the middle of the talc-sand block at an angle of 45° to the principal compression direction (σ_1). Type 1 experiments were performed in multiple sets by varying the sand:talc volume ratio-**

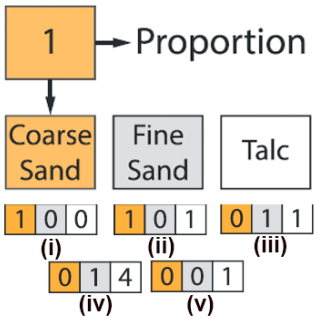

(i) 1:0 (pure coarse sand),

(ii) 1:1 (coarse sand-talc mixture),

(iii) 1:1 (fine sand-talc mixture),

(iv) 1: 4 (fine sand-talc mixture), and

(v) 0:1 (pure talc).

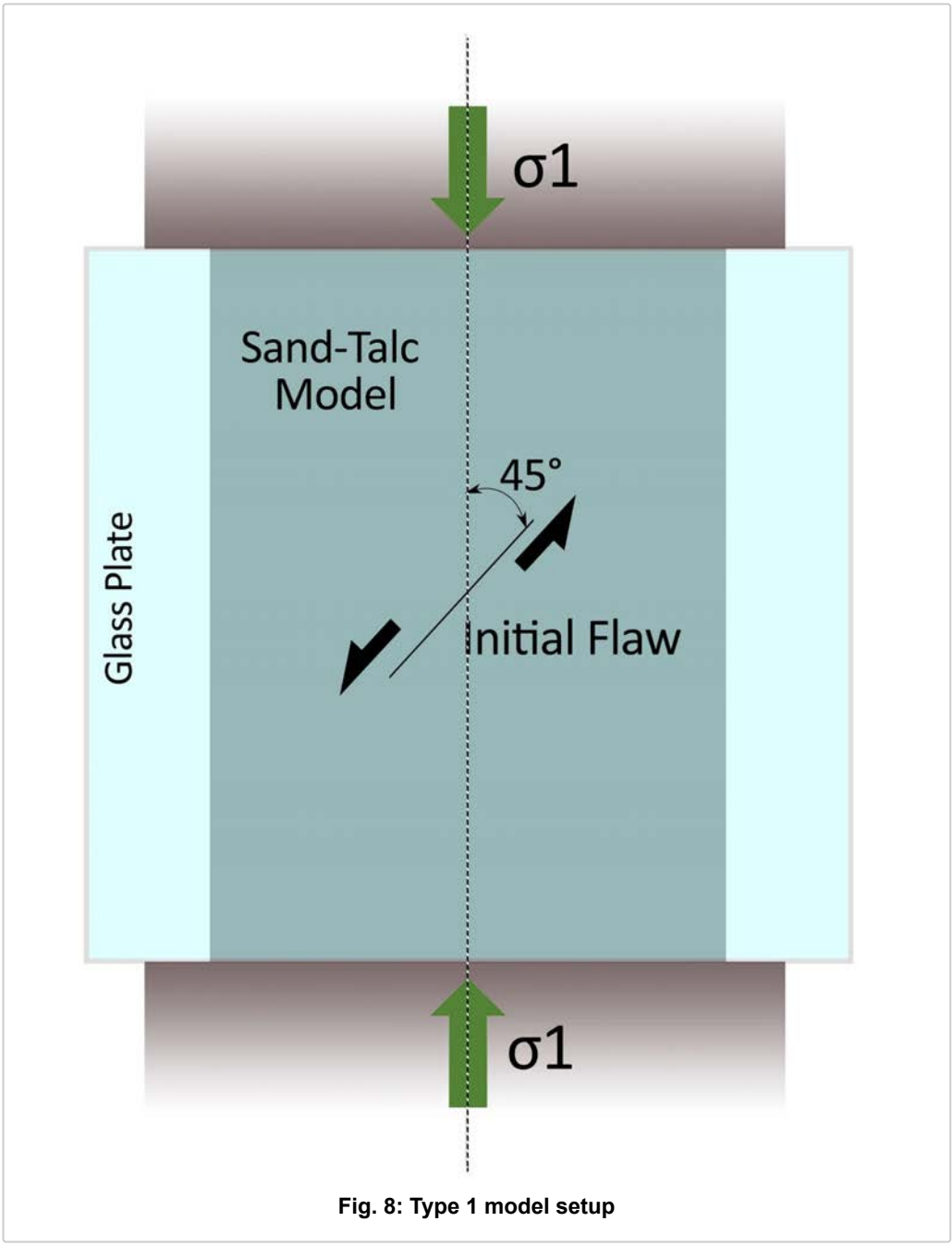

Fig. 8: Type 1 model setup

- **Type 2 Model: The model had a throughgoing cut, which activated to produce a shear fracture during the compression. The model block was prepared by using only talc, added with cement and water. The block was cut into two halves at the desired angle (θ) to the principal compressive stress axis (σ_1).**

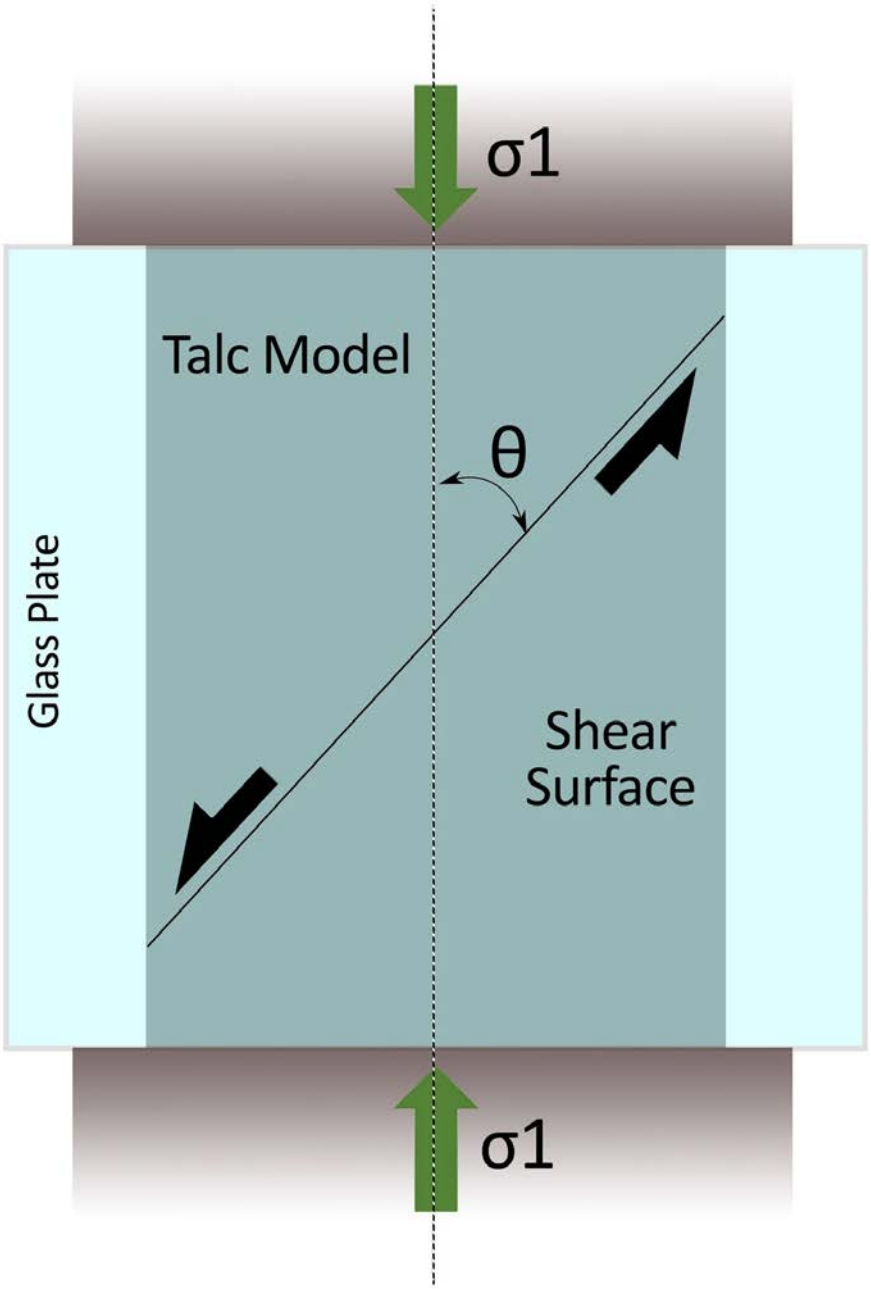

Fig. 9: Type 2 model setup

EXPERIMENTAL FINDINGS

Type 1 Experimental Results

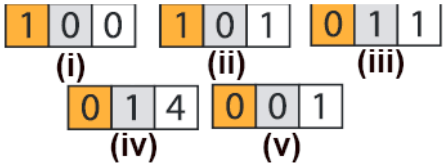

(i) Produced excellent shear fractures but without any prominent linear features on them (*Fig. 10a*).

(ii) Also did not develop typical slickensides but showed weak traces of slip motion, albeit locally on the shear fractures. (*Fig. 10b*).

(iii) Yielded multiple sets of shear fractures with somewhat discernible linear irregularities (*Fig. 10c*).

(iv) Produced shear fractures with bold slickenlines, localized in isolated patches (*Fig. 10d*).

(v) Produced excellent one-dimensional irregularities, giving an appearance of typical slickensides (*Fig. 10e*)

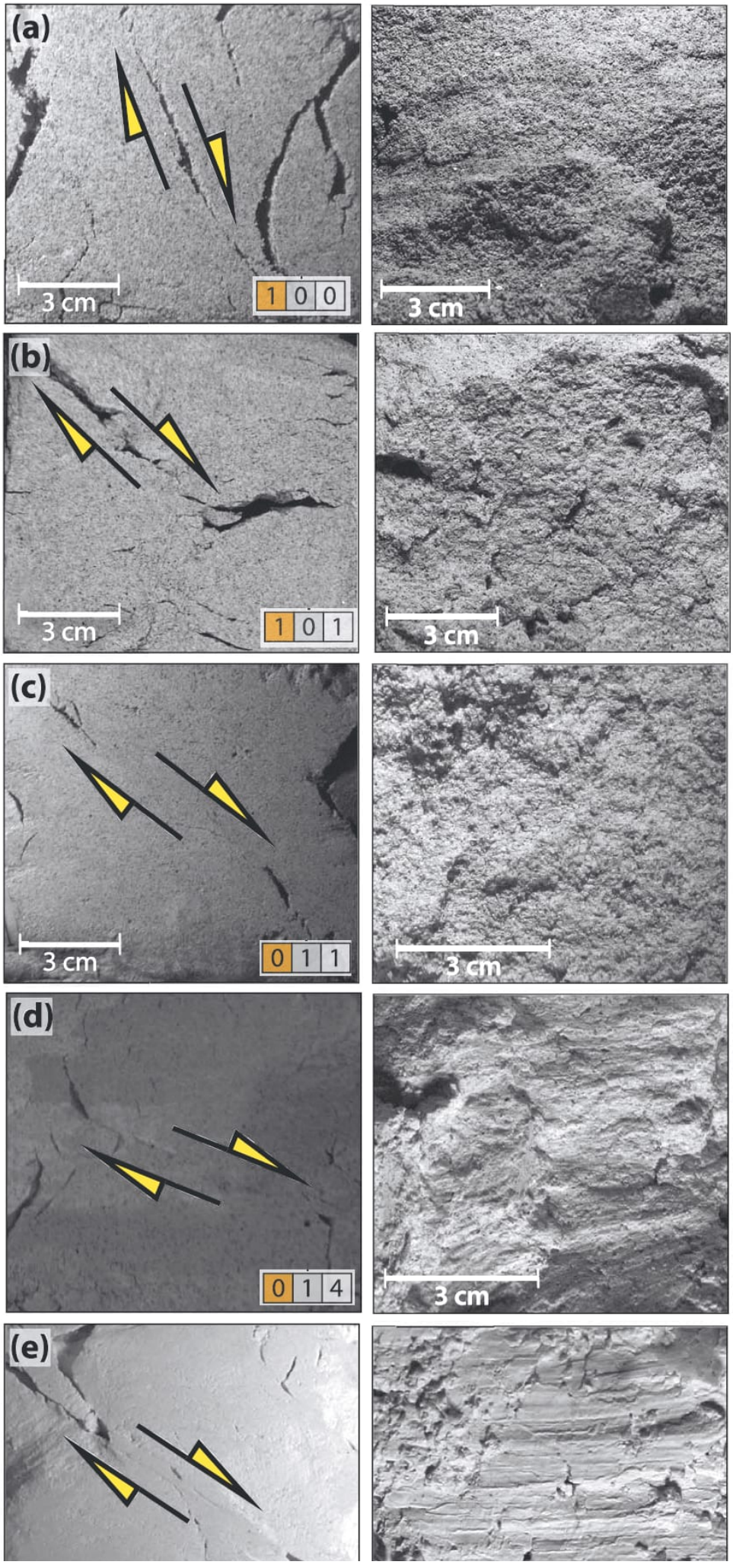
(a)
3 cm
1 0 0
3 cm
(b)
3 cm
1 0 1
3 cm
(c)
3 cm
0 1 1
3 cm
(d)
0 1 4
3 cm
(e)

Type 2 Experimental Results

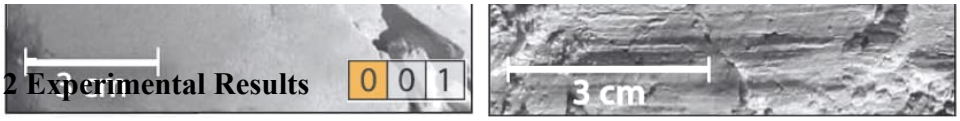

Fig. 10: Formation of shear fractures in Type 1 sand-talc models (left panel) under laboratory conditions (top views). (a) Pure sand, (b) coarse sand-talc (1:1) (c) fine sand-talc (1:1); (d) fine sand-talc (1:4) and (e) pure talc. Their corresponding

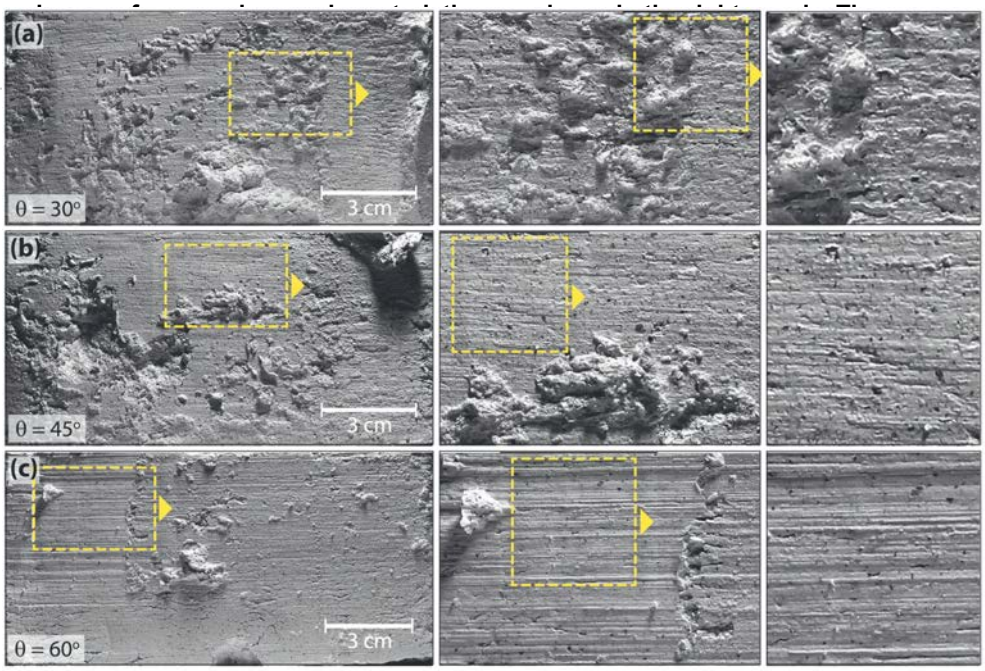

Fig. 11: Variations of the shear fracture roughness in Type 2 pure talc models. The shear fracture angles to the compression direction (θ) were (a) 30°, (b) 45°, and (c) 60°. Notice that the shear surfaces contain relatively smooth domains with prominent lineation (slip zones) and rough domains without any linearity (stuck zones). The latter tends to die out with increasing θ. The yellow boxes show areas of observation with successive magnifications (left to right).

ROUGHNESS ANALYSIS

Computational Method

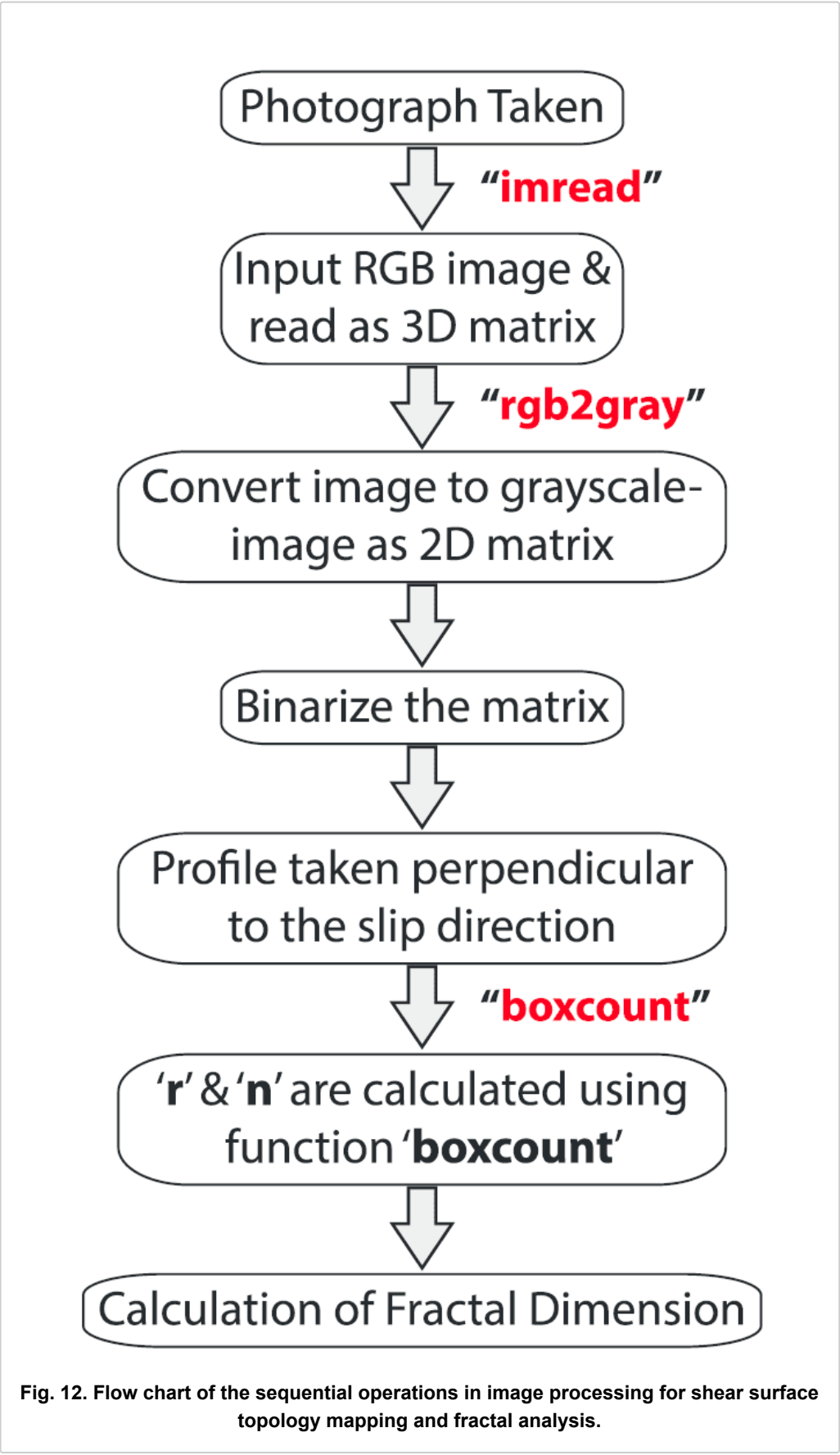

Fig. 12. Flow chart of the sequential operations in image processing for shear surface topology mapping and fractal analysis.

Analysis Results

Casts Analysis

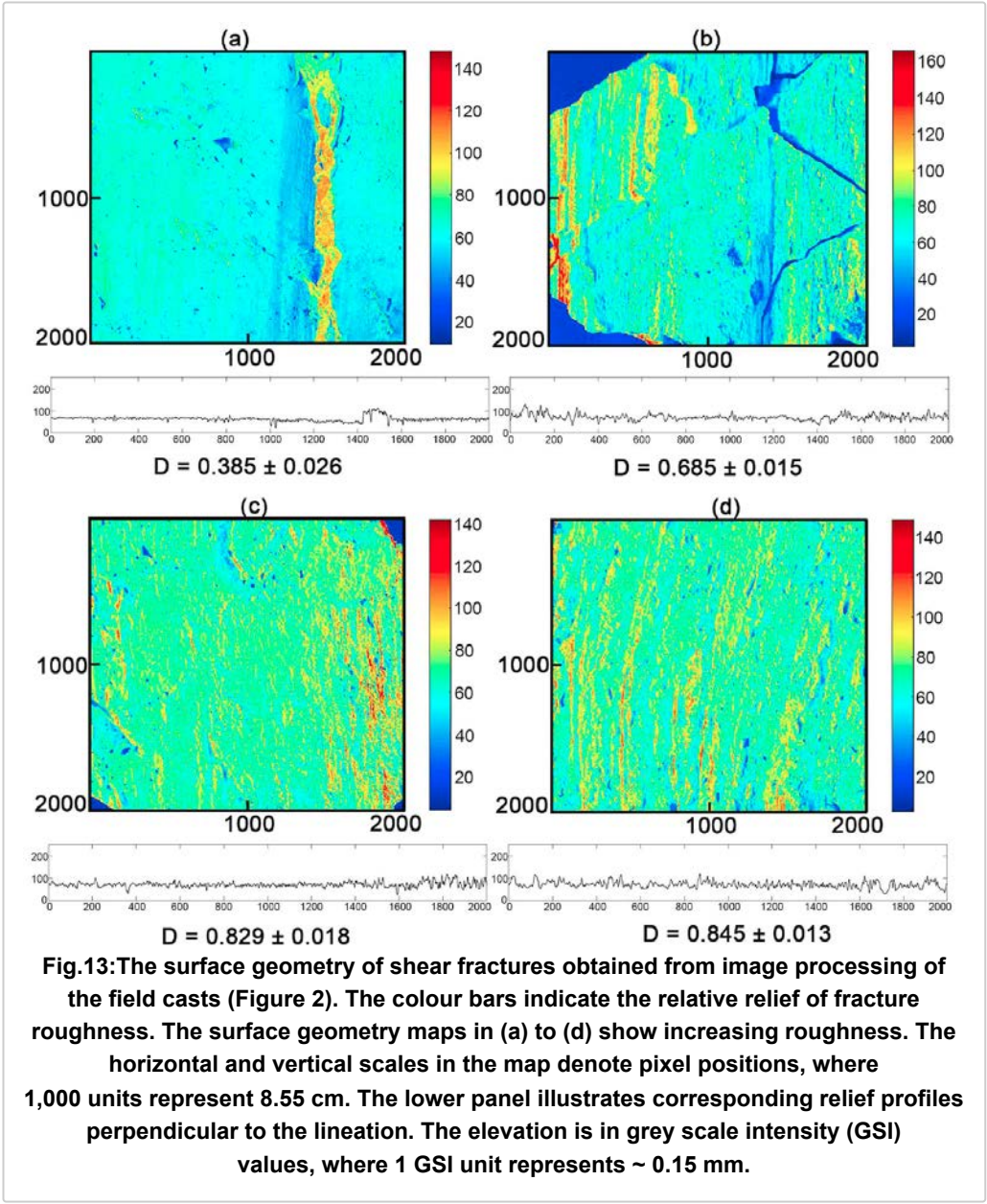

Fig.13:The surface geometry of shear fractures obtained from image processing of the field casts (Figure 2). The colour bars indicate the relative relief of fracture roughness. The surface geometry maps in (a) to (d) show increasing roughness. The horizontal and vertical scales in the map denote pixel positions, where 1,000 units represent 8.55 cm. The lower panel illustrates corresponding relief profiles perpendicular to the lineation. The elevation is in grey scale intensity (GSI) values, where 1 GSI unit represents ~ 0.15 mm.

Type 1 Experiment Analysis

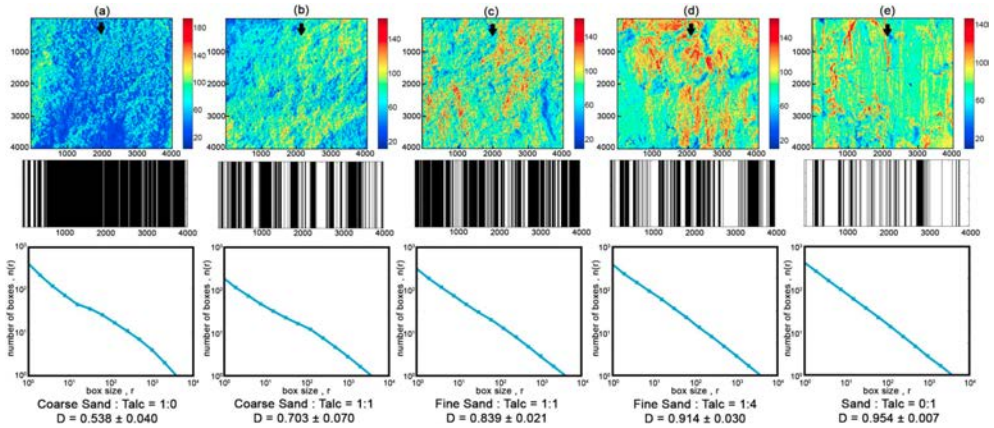

Fig. 14: The roughness geometry of experimental shear fractures is shown in Figure 4. (a) Pure sand, (b) coarse sand-talc (1:1); (c) fine sand-talc (1:1); (d) fine sand-talc (1:4) and (e) pure talc. The horizontal and vertical scales in the map denote pixel positions, where 1,000 units represent 8.55 cm. The images (a to e) reveal increasing linearity in roughness. The corresponding cantor set and fractal analyses are presented in the lower panels. D: one-dimensional fractal dimension. The arrows indicate the slip motion of the top walls.

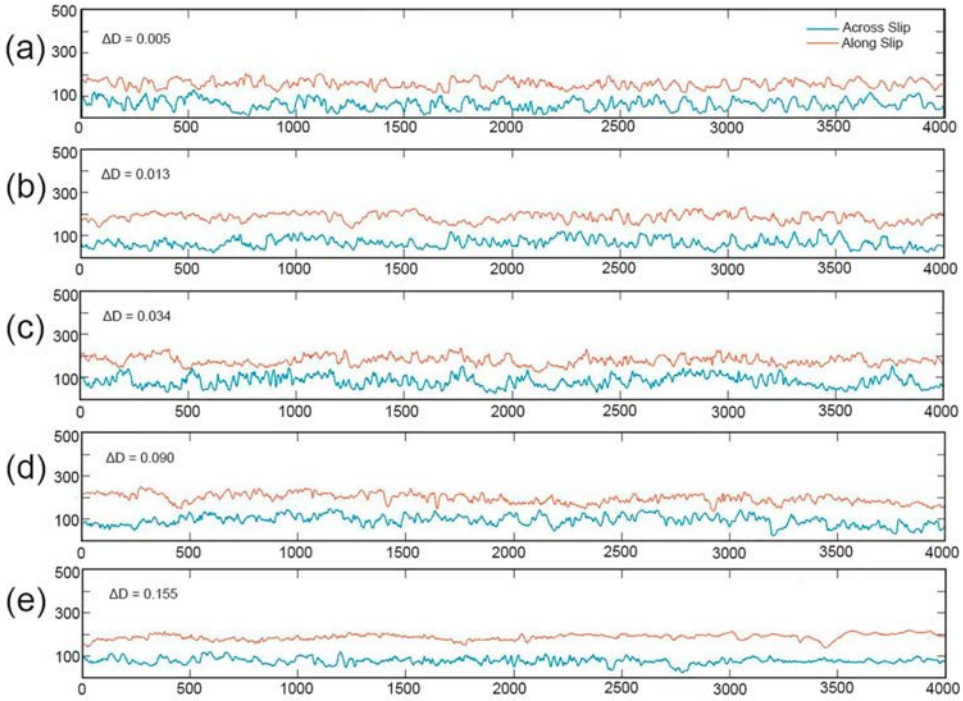

Fig. 15: Across- and along-slip roughness profiles obtained from the surface geometry maps (Figure 8) of shear fractures produced in Type 1 laboratory experiments (the two graphs are plotted at a given spacing). (a–e) Sand:talc models with increasing talc content, as shown in Figure 4. ΔD is the difference in fractal dimensions estimated across and along the slip direction. Note the increasing ΔD from (a) to (e), implying stronger anisotropy in roughness from sand to talc models. The horizontal scale is in pixel position (1,000 units = 8.55 cm), and the vertical scale in GSI values (1 unit ~ 0.15 mm).

Type 2 Experiment Analysis

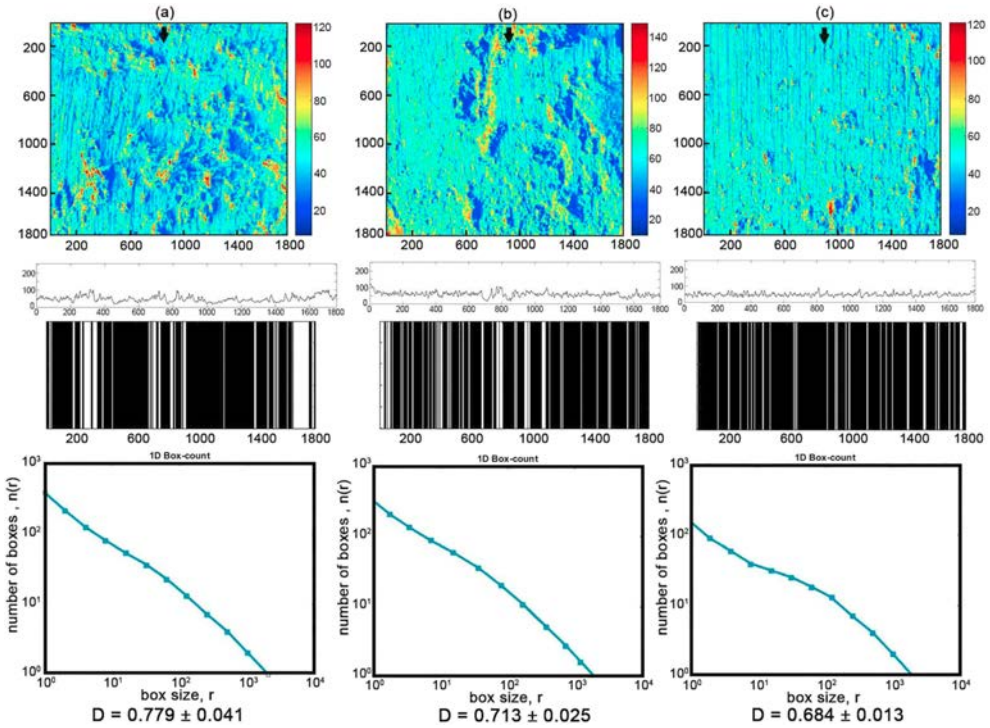

Fig. 16: Effects of the initial fracture orientation (θ) on the surface roughness in Type 2 experiments. *θ* = (a) 30°, (b) 45,° and (c) 60°. *θ*: Inclination of the fractures to the principal compression direction. The corresponding across-slip profiles, cantor sets, and fractal analysis are shown below.

FIELD STUDY

Field Area

Southern parts of the Singhbhum Shear Zone and some adjoining parts of the Singhbhum Fold Belt on the north of SSZ (*Fig. 3*). Two locations were chosen: (1) Patherogora region near old Surda copper mines and (2) Tentuldanga region. Patherogora is a small village in Purbi Singhbhum district, Jharkhand (22°32′37.911″N, 86°26′31.223″E, altitude: 146 m, accuracy: ±3 m), and falls in the southern part of SSZ.

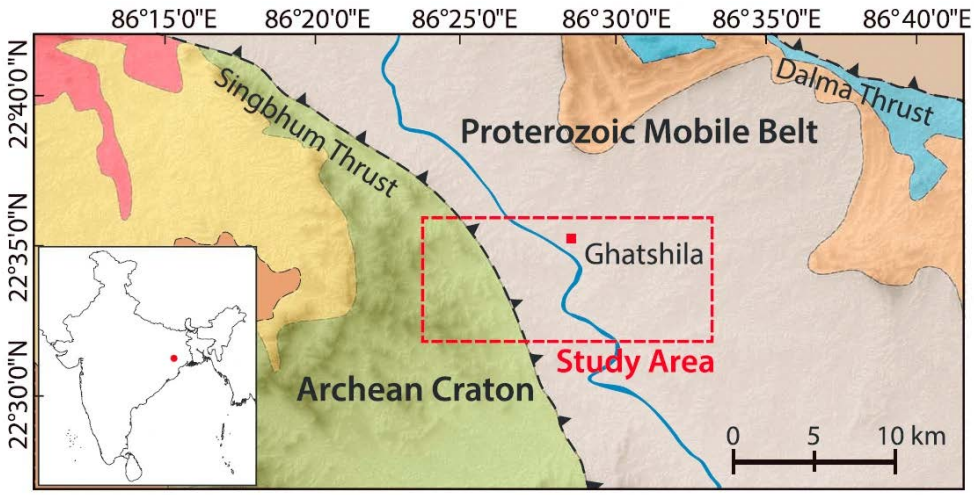

Fig. 3: Location map of the Precambrian Singhbhum Craton in eastern India (shown as inset). Our study area is indicated with the red box at the south eastern flank of Singhbhum Shear Zone (SSZ).

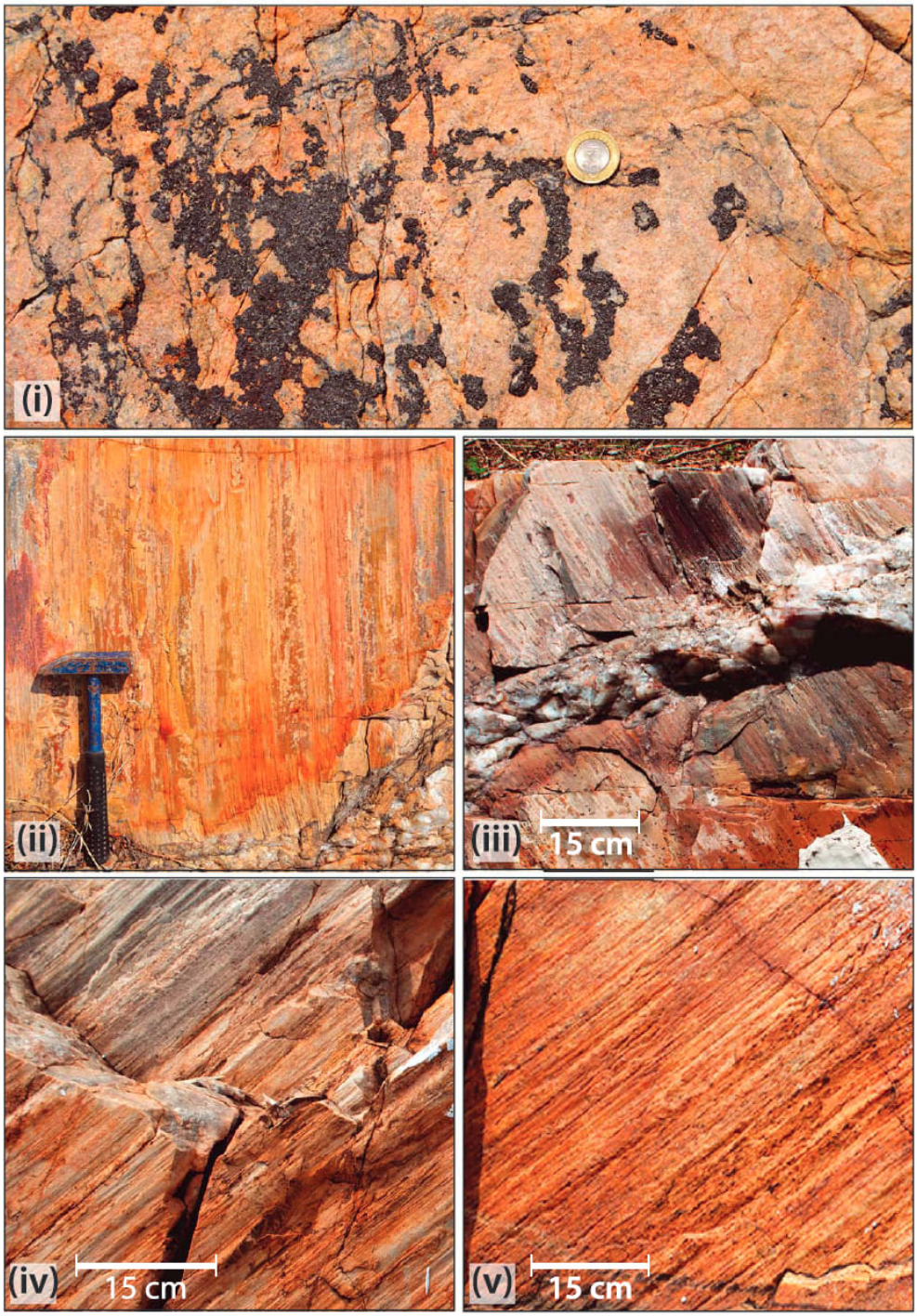

Fig. 4: Three principal types of slickensides observed in the SSZ area. (i) Type 1: Smooth fault surfaces without any discernible linear roughness; (ii and iii) Type 2: slickensides with lineation defined by fine-scale ridges and grooves; and (iv and v) Type 3: slickensides with wavy linear roughness defined by ridges and grooves of varying coarseness. The coin diameter (i) and hammer length (ii) are 2.7 and 30 cm, respectively.

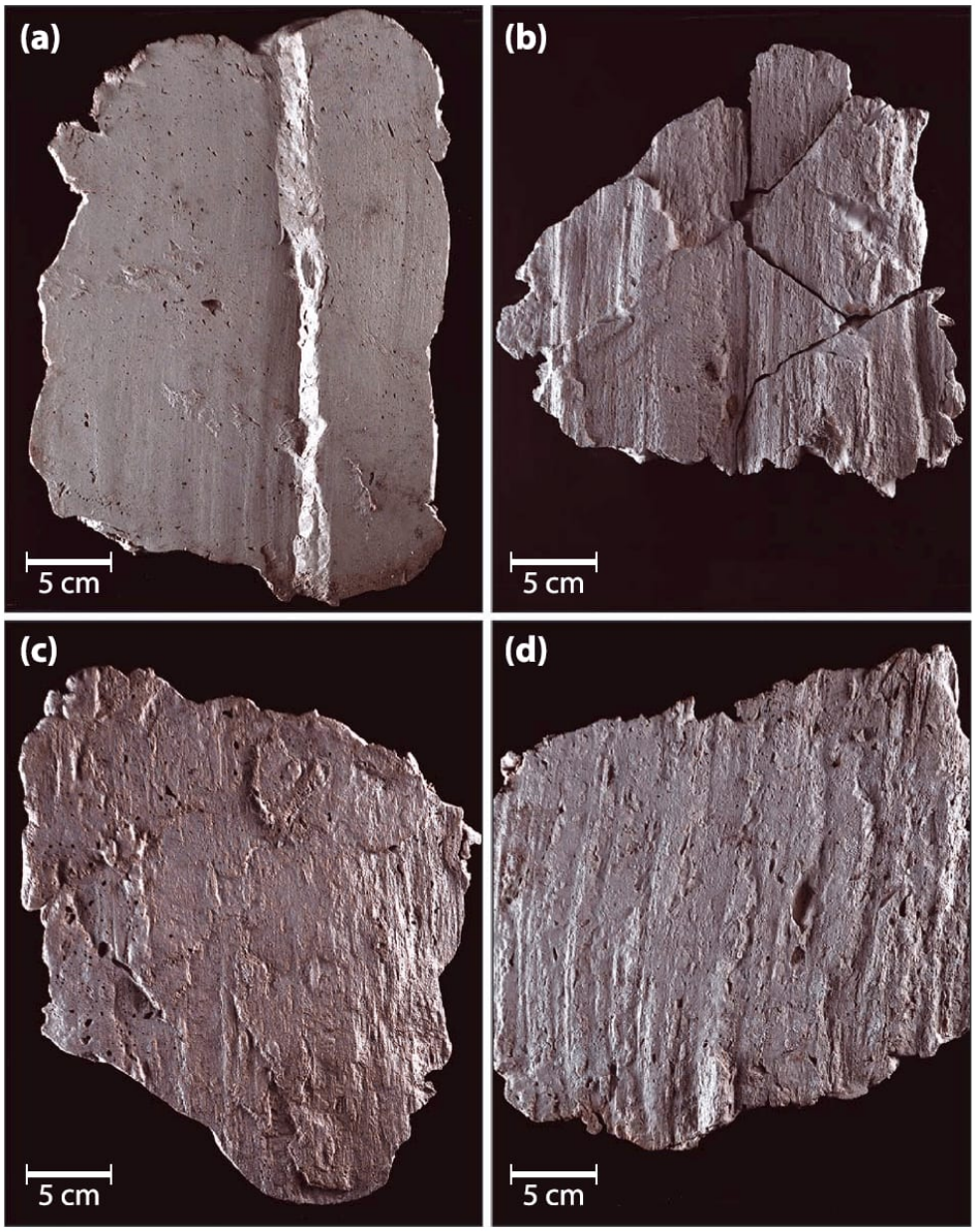

Fig. 5: Casts of slickensides with varying roughness from the field. (a) Smooth shear surfaces, but with down-dipping, low-amplitudes waves, forming a distinct fine scale slickenline structure. (b) Shear surfaces with strongly linear roughness, defined by cylindrical ridges and grooves in different orders. (c) Shear surfaces with heterogeneous linear roughness. There are patchy zones showing weak linearity in the roughness. (d) Shear surface roughness with wavy appearance of long ridges and grooves at varying spacing.

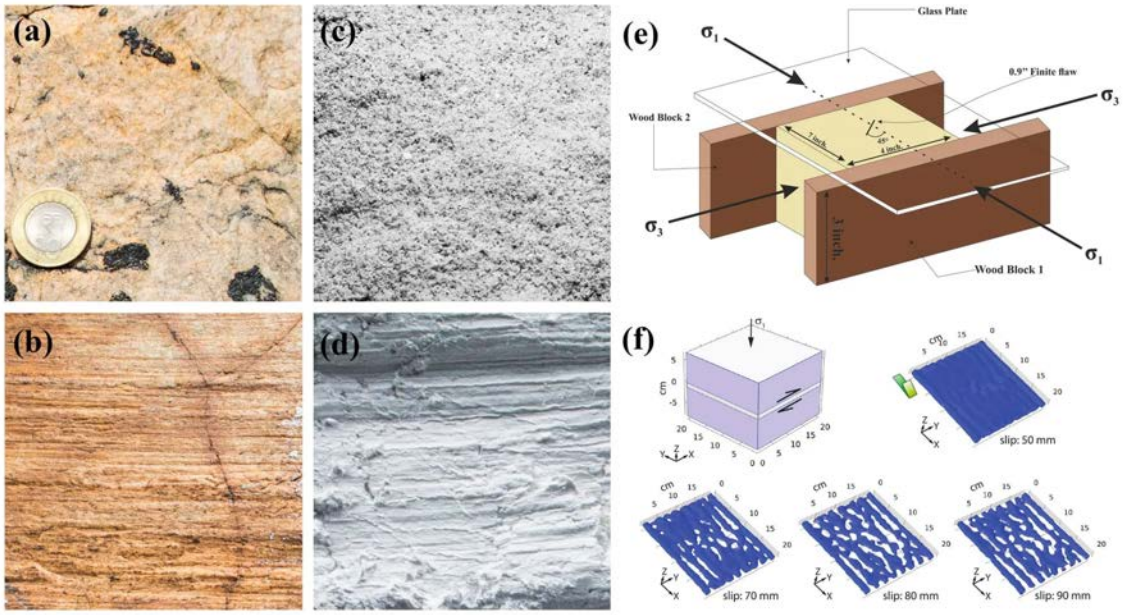
(a)
(c)
(e)
(b)
(d)
(f)
Glass Plate
0.9" Finite flaw
Wood Block 2
Wood Block 1
3 inch.
slip: 50 mm
slip: 70 mm
slip: 80 mm
slip: 90 mm

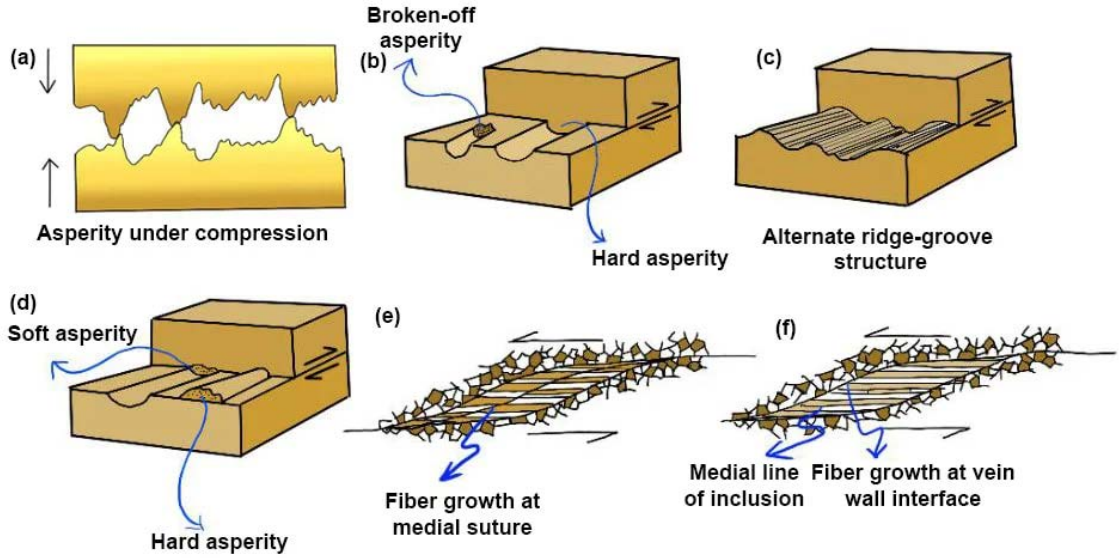
(a)
Asperity under compression
Broken-off asperity
(b)
Hard asperity
(c)
Alternate ridge-groove structure
(d)
Soft asperity
Hard asperity
(e)
Fiber growth at medial suture
(f)
Medial line of inclusion
Fiber growth at vein wall interface

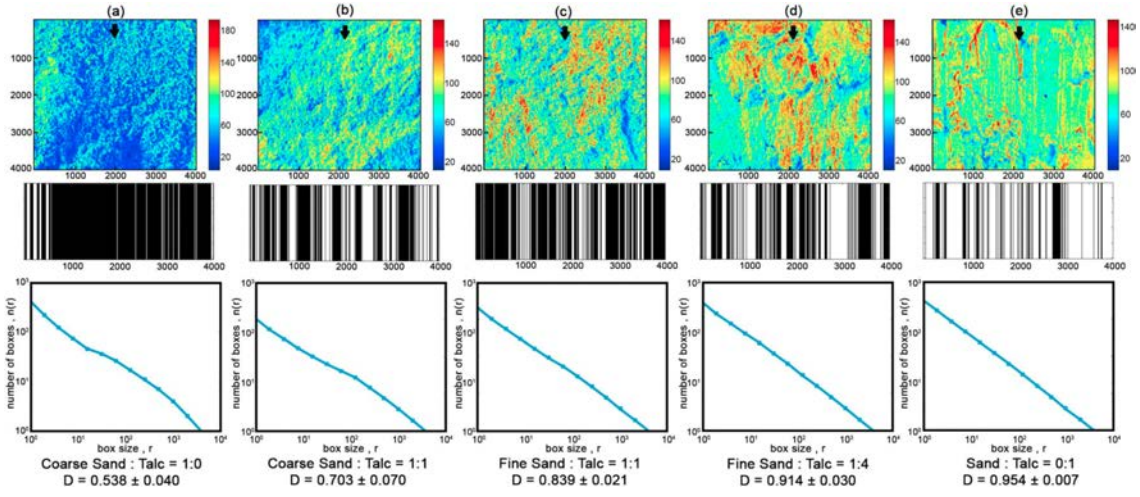
(a)
(b)
(c)
(d)
(e)
number of boxes , n(r)
box size , r
Coarse Sand : Talc = 1:0
D = 0.538 ± 0.040
Coarse Sand : Talc = 1:1
D = 0.703 ± 0.070
Fine Sand : Talc = 1:1
D = 0.839 ± 0.021
Fine Sand : Talc = 1:4
D = 0.914 ± 0.030
Sand : Talc = 0:1
D = 0.954 ± 0.007

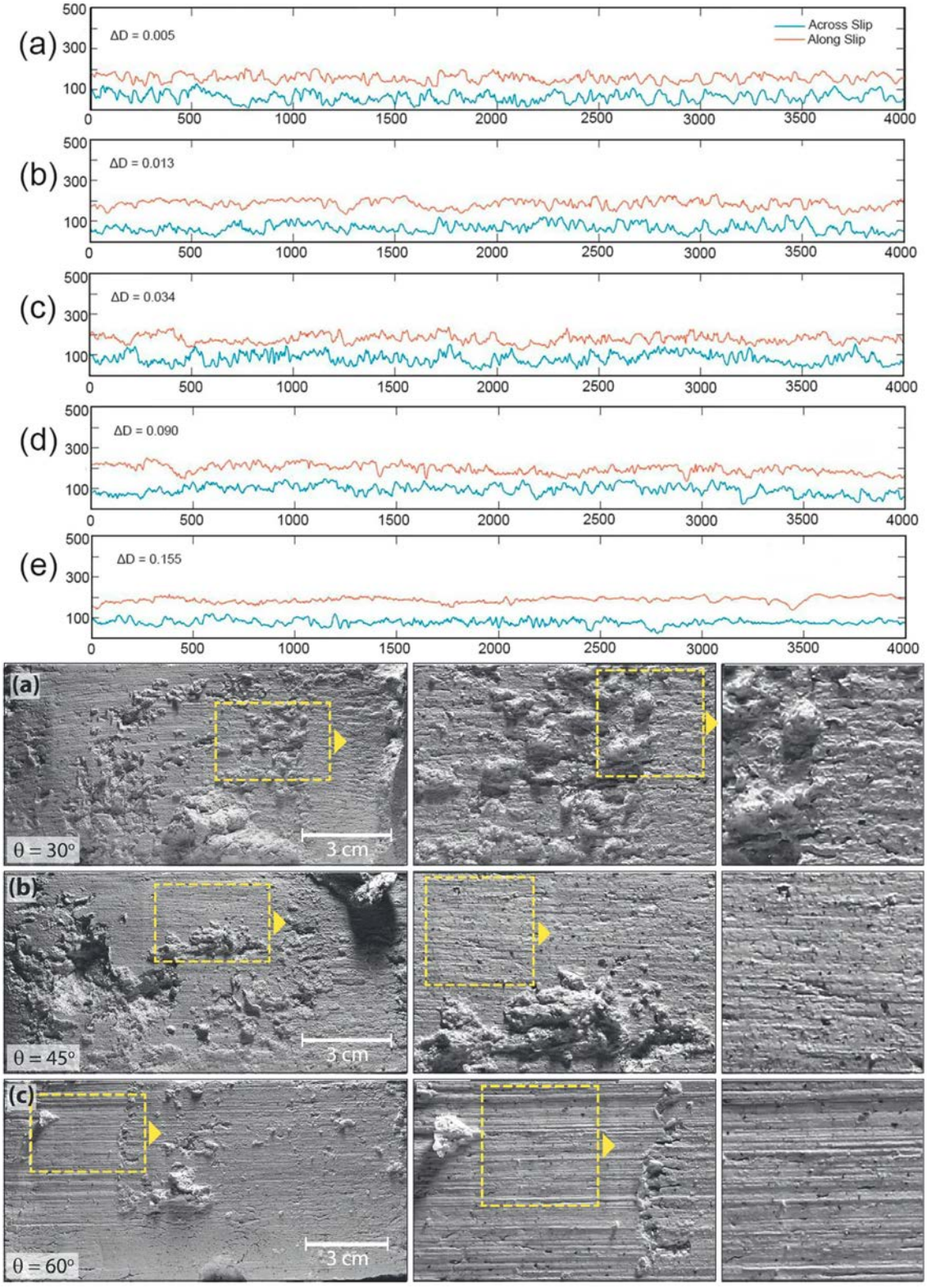
(a)
ΔD = 0.005
Across Slip
Along Slip
(b)
ΔD = 0.013
(c)
ΔD = 0.034
(d)
ΔD = 0.090
(e)
ΔD = 0.155
500
300
100
0
500
1000
1500
2000
2500
3000
3500
4000
(a)
θ = 30°
3 cm
(b)
θ = 45°
3 cm
(c)
θ = 60°
3 cm

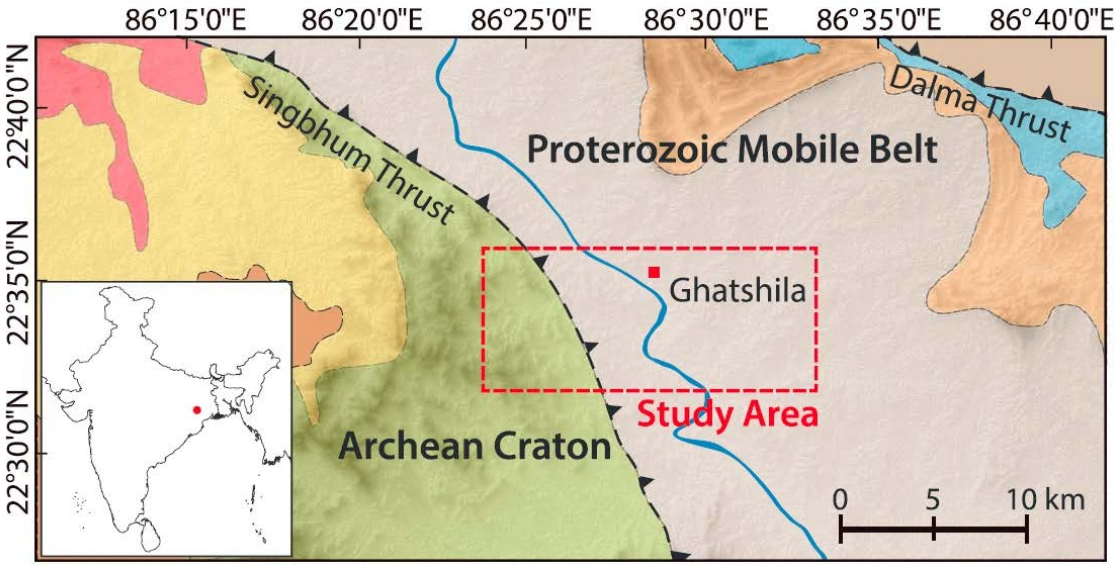

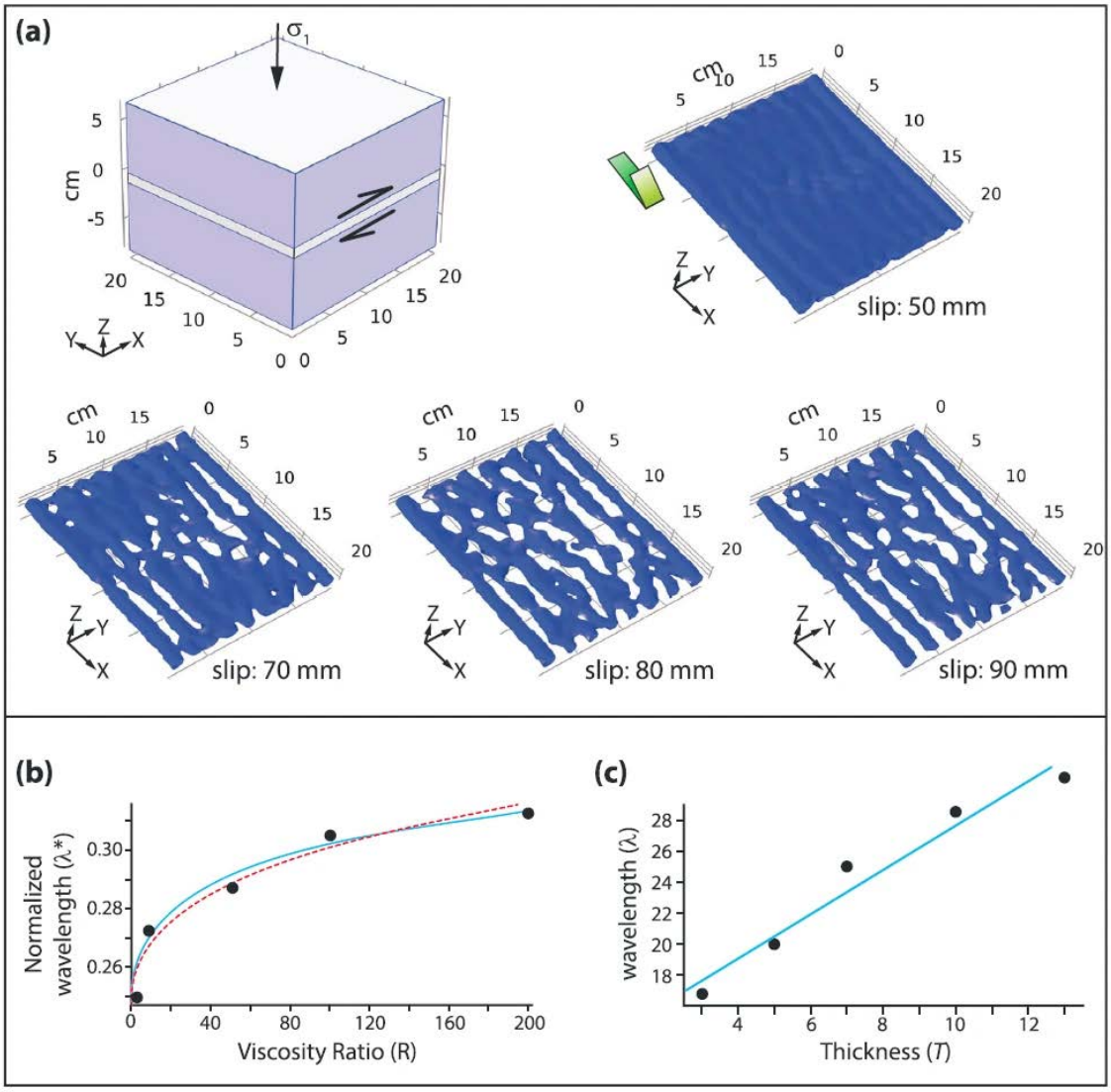

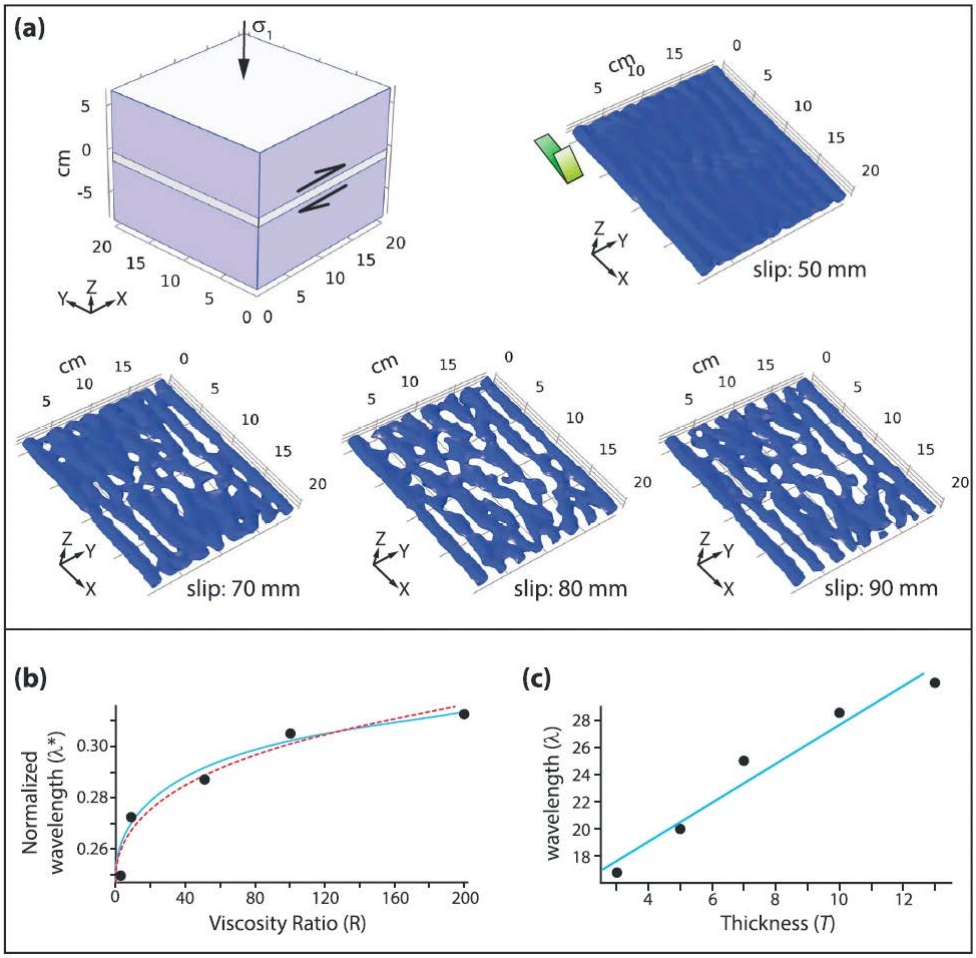

Fig. 17: (a) 3-D computational fluid dynamic (CFD) model used for investigation of shear instability in a low-viscosity layer sandwiched between two high-viscosity blocks (viscosity ratio: 10^2) and successive stages of instability wave growth, leading to the along-slip ridge and groove structures, as observed in pure talc models (*Fig. 10e*). The model was subjected to slip movement along the soft zone. σ1 indicates the normal stress to the slip zone. (b) Calculated plots of normalized wavelength ($\lambda^* = \lambda/T$) with viscosity ratio (R). The nonlinear variation (blue line) closely follows a cubic root function of *R* (red dashed line). (c) The linear variation of *λ* with *T*.

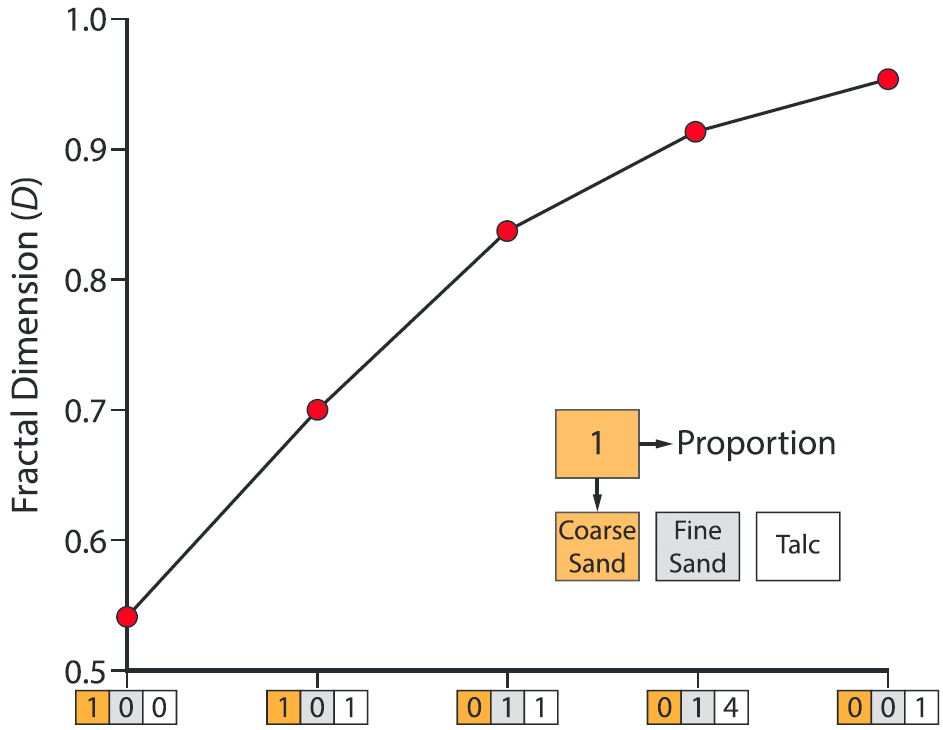

Fig. 18: Calculated plot of the fractal dimension (D) as a function of the sand-talc volume proportions (shown in the corresponding boxes) in experimental models. With increasing talc content, the transition of Coulomb failure to plastic yielding leads to more prominent linearity in the roughness from shear fractures.

Conclusion

1. Shear surfaces in the field show mainly three types of roughness patterns: Type 1—smooth surfaces without any distinct linear irregularities, Type 2—linear roughness with fine scale ridges of small amplitudes, and Type 3—linear roughness with coarse ridges of relative large amplitudes.

2. The mode of failure and the initial inclination of fractures to the principal compression direction are the potential factors in controlling the linear roughness of shear surfaces.

3. Increase in θ promotes the formation of smooth slickenlines at the cost of rough zones.

4. Increasing ductility promotes ΔD values.

5. Mechanical instability is a potential mechanism for roughness formation with marked linearity in the slip zones.

AUTHOR INFORMATION

Uddalak Biswas[1,2]

Prof. Nibir Mandal[1]

Manaska Mukhopadhyay[1]

[1]Department of Geological Sciences, Jadavpur University, Kolkata, West Bengal, India 700032

[2]Structural Geology Lab., Department of Earth Sciences, Indian Institute of Engineering Science and Technology, Shibpur, Howrah, West Bengal, India 711103

ABSTRACT

Slickenlines (linear marks) on fault surfaces are the most common indicator of fault slip events. From sheared quartzite in the Singhbhum Shear Zone, eastern India, this study reports varying slip surface roughness (smooth without lineation to strongly rough with intense lineation) imparted by slickenlines. Analogue experiments with sand-talc models suggest that the modes (brittle versus ductile) of shear failure and the inclination of pre-existing slip planes to principal stress direction (θ) largely control the roughness characteristics of a fault surface. Coulomb failure in pure sand models in the brittle regime produces a smooth fault surface with little or no slickenlines roughness features. On the other hand, increasing talc content in the models resulted in a transition from brittle to ductile shear failure, and slip surfaces produced prominent slickenlines in the slip direction that becomes strong with increasing θ= 30° to 60°. This study provides a roughness analysis of the laboratory models and field casts in terms of 1D fractal dimension (D) using the box-counting method and the image processing technique. The directionality in D, measured as ΔD (difference in D across and along the slip direction), is evaluated to show the degree of roughness anisotropy on slip surfaces. The present work also sheds light upon the origin of slickenlines. Previous workers hypothesized them as a product of ploughing action by asperities, directional deposition of the abraded asperities, and syn-kinematic growth of secondary minerals. This study introduces a new interpretation, showing slip-induced wave instability as a possible mechanism of slickenlines formation.

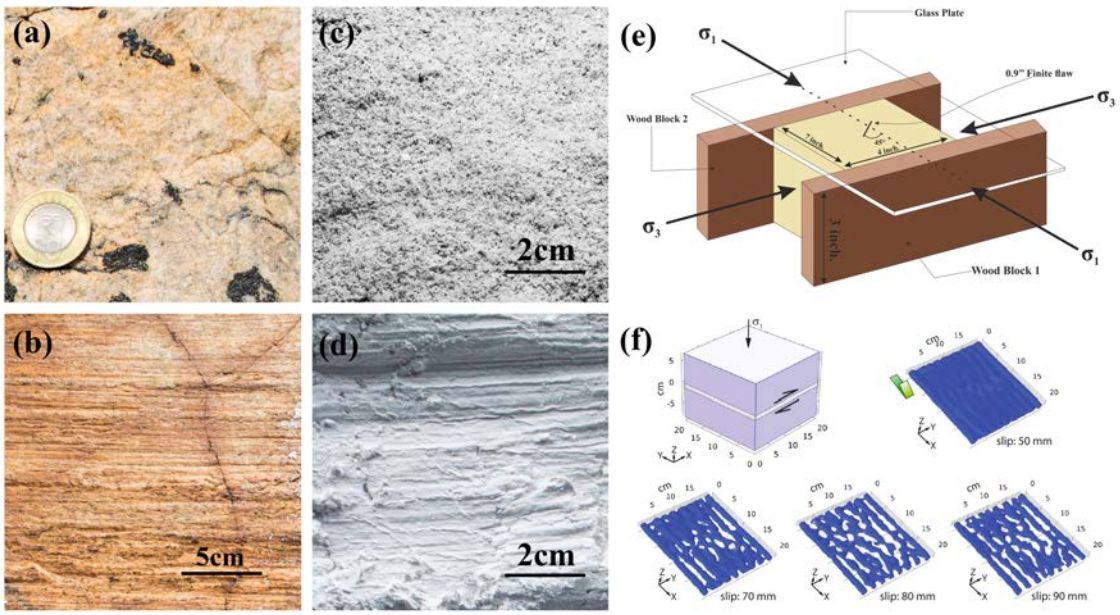

(a) Smooth natural fault surface without any lineation (coin diameter 2.6 cm), (b) Natural fault plane with prominent slickenlines, (c) Model fault surface devoid of any slickenlines, (d) Model shear surface with visible lineation, (e) Laboratory model setup of shear surface simulation, (f) Numerical model with progressive slip.

(https://agu.confex.com/data/abstract/agu/fm22/7/6/Paper_1054167_abstract_955126_0.jpg)

REFERENCES

Means, W. D. (1987). A newly recognized type of slickenside striation. Journal of Structural Geology, 9(5–6), 585–590. https://doi.org/10.1016/0191-8141(87)90143-X

Mukhopadhyay, M., Biswas, U., Mandal, N., & Misra, S. (2019). On the development of shear surface roughness. Journal of Geophysical Research: Solid Earth, 124. https://doi.org/10.1029/2018JB016677

Twiss, R., & Moores, E. (1992). Structural geology. New York: W. H. Freeman Publications.